Metasurface-Based Hybrid Optical Cavities for Chiral Sensing

Nico S. Baßler,[1,2] Andrea Aiello,[1] Kai P. Schmidt,[2] Claudiu Genes,[1,2] and Michael Reitz[1,3]
[1]Max Planck Institute for the Science of Light, D-91058 Erlangen, Germany
[2]Department of Physics, Friedrich-Alexander-Universität Erlangen-Nürnberg (FAU), D-91058 Erlangen, Germany
[3]Department of Chemistry and Biochemistry, University of California San Diego, La Jolla, California 92093, USA

(Received 13 June 2023; accepted 21 December 2023; published 25 January 2024)

Quantum metasurfaces, i.e., two-dimensional subwavelength arrays of quantum emitters, can be employed as mirrors towards the design of hybrid cavities, where the optical response is given by the interplay of a cavity-confined field and the surface modes supported by the arrays. We show that stacked layers of quantum metasurfaces with orthogonal dipole orientation can serve as helicity-preserving cavities. These structures exhibit ultranarrow resonances and can enhance the intensity of the incoming field by orders of magnitude, while simultaneously preserving the handedness of the field circulating inside the resonator, as opposed to conventional cavities. The rapid phase shift in the cavity transmission around the resonance can be exploited for the sensitive detection of chiral scatterers passing through the cavity. We discuss possible applications of these resonators as sensors for the discrimination of chiral molecules. Our approach describes a new way of chiral sensing via the measurement of particle-induced phase shifts.

DOI: 10.1103/PhysRevLett.132.043602

Conventional isotropic (e.g., metallic) mirrors reverse the handedness (or helicity) of circularly polarized light by turning right-circularly polarized (RCP) light into left-circularly polarized (LCP) light and vice versa [1–3]. This makes it impossible to realize helicity-preserving (HP) cavities or even chiral cavities (i.e., cavities only supporting light modes of a certain handedness), with conventional mirrors [4]. There is, however, a great current scientific and technological interest in the design of HP or chiral mirrors, metasurfaces, and resonators [5–11], in particular, for the enhancement of so-called dichroic effects. Dichroism refers to the (typically weak) differential absorption of circularly polarized light by chiral scatterers such as molecular enantiomers [12]. Enhancing dichroic effects with optical resonators can result in better sensitivities for the discrimination of molecular enantiomers [13–17], a desired task for biochemical applications. Other techniques for chiral sensing include measurements of photoelectron circular dichroism (PECD) [18], three- or multiwave mixing [19,20], or chirality-induced spin selectivity (CISS) [21]. In the strong light-matter coupling regime, chiral cavities have recently been proposed to create novel light-dressed states of matter by breaking the time-reversal symmetry in materials, leading to the emerging field of chiral polaritonics [22,23]. In this Letter, we show that HP cavities can be implemented with quantum metasurfaces employed as mirrors. These structures have emerged as platforms for achieving strong and highly directional light-matter interactions and can most prominently be realized with cold atoms trapped in optical lattices [24]. They can exhibit close to perfect reflection of incoming light [24–29] and have numerous other applications, e.g., as platforms for topological quantum optics [30–32], nonlinear quantum optics [33–38], or quantum information processing [39–44]. The main ingredient of our approach is to manipulate the polarization of the incoming light field via the orientation of the effective two-level systems that make up the metasurfaces, which can, for instance, be tuned via an external magnetic field for certain atomic transitions. We, however, strongly emphasize that our treatment is in principle valid for any array of point dipoles and could be analogously implemented with arrays of classical dipoles such as plasmonic lattices, in which case no external magnetic field control is needed as the polarization can be controlled by the geometry of the individual elements [45].

More generally, this work falls within the scope of *hybrid cavities*, i.e., the design of optical resonators going beyond the simple textbook picture of a single electromagnetic mode confined between two nonreactive mirrors. Instead, strongly dispersive optical elements such as photonic crystals or plasmonic metasurfaces are used as reflectors [46–50] with the aim to surpass the performance of standard cavities, implying a highly non-Markovian behavior of the cavity as characterized by non-Lorentzian, typically Fano-type line shapes [51].

HP mirror.—Let us present an implementation procedure for a HP mirror using a stacked system of quantum metasurfaces. We start by introducing the formalism for a single metasurface [52]. To this end, we consider a 2D quasi-infinite quantum emitter array comprised of $\mathcal{N}$ emitters at transition frequency ω_0 situated in the xy plane at positions $\mathbf{r}_j$. For simplicity, one may imagine a square lattice; however, most of the results derived in the following are equally valid for other Bravais lattices. For the HP mirror, in the following we require that the transition dipoles of the emitters in the array can be identically oriented along a certain direction. One possible implementation of this lies in employing the magnetic substructure of a $J = 0 \to J = 1$ transition [24,37]. In the Cartesian polarization basis, the transition dipole operator for each emitter can then be written as $\mathbf{d} = \sum_\nu \mathbf{d}_\nu \sigma_\nu + \text{H.c.}$ with $\mathbf{d}_\nu = \langle g|\mathbf{d}|\nu\rangle$, and $\sigma_\nu = |g\rangle\langle\nu|$ is the corresponding lowering operator for each electronic transition ($\nu = x, y, z$). An external magnetic field along the ν direction can be used to "select" the ν-transition dipole (by making all other transitions orthogonal to the magnetic field off-resonant [52]). Other implementations could rely on artificial, nanoprinted elements (see previous work [53]), photonic crystal mirrors [49], or solid-state platforms [54]. We consider a laser drive entering from the left in the form of a plane wave with positive-frequency amplitude $\mathbf{E}_{\text{in}}^{(+)} = (E_{\text{in},x}, E_{\text{in},y}, 0)^\top$ and laser frequency $\omega_l = 2\pi c/\lambda = ck_l$, where λ and k_l are the laser wavelength and wave number, respectively.

In a frame rotating at the laser frequency, the Hamiltonian describing the dynamics of the emitter array is given by the sum of the free evolution and the dipole-dipole interaction ($\hbar = 1$)

$$\mathcal{H}_0 + \mathcal{H}_{\text{d-d}} = -\Delta \sum_{j,\nu} \sigma_{j,\nu}^\dagger \sigma_{j,\nu} + \sum_{j,j',\nu,\nu'} \Omega_{jj'}^{\nu\nu'} \sigma_{j,\nu}^\dagger \sigma_{j',\nu'}, \quad (1)$$

with the laser detuning $\Delta = \omega_l - \omega_0$ and $\sigma_{j,\nu}$ the lowering operator for the ν transition within a particular emitter j. Assuming normally incident illumination, the laser drive adds as $\mathcal{H}_l = \sum_{j,\nu}(\eta_\nu \sigma_{j,\nu}^\dagger + \text{H.c.})$ with Rabi frequencies $\eta_\nu = d_\nu E_{\text{in},\nu}^{(+)}$ and $\eta_z = 0$. In addition to the coherent processes, the collective loss of excitations due to spontaneous emission is described by the Lindblad term

$$\mathcal{L}[\rho] = \sum_{j,j',\nu,\nu'} \Gamma_{jj'}^{\nu\nu'} \left[\sigma_{j,\nu} \rho \sigma_{j',\nu'}^\dagger - \frac{1}{2}\{\sigma_{j,\nu}^\dagger \sigma_{j',\nu'}, \rho\}\right], \quad (2)$$

where the last term denotes an anticommutator and the diagonal elements describe the independent spontaneous emission of the emitters $\Gamma_{jj}^{\nu\nu'} = \Gamma_0 \delta_{\nu\nu'}$ with $\Gamma_0 = \omega_0^3 d^2/(3\pi\epsilon_0 c^3)$ (we assume the dipole moments to be identical in the following $d_\nu \equiv d$). The rates $\Omega_{jj'}^{\nu\nu'}$, $\Gamma_{jj'}^{\nu\nu'}$ describe coherent or incoherent scattering of photons between emitters j and j' and between transitions ν and ν' and can be derived as real and imaginary parts of the photonic Green's tensor (see Supplemental Material [55]) as

$$\Omega_{jj'}^{\nu\nu'} - \mathrm{i}\frac{\Gamma_{jj'}^{\nu\nu'}}{2} = -\mu_0 \omega_0^2 \mathbf{d}_\nu^* \cdot \mathbf{G}(\mathbf{r}_{jj'}) \cdot \mathbf{d}_{\nu'}, \quad (3)$$

expressed in terms of the vacuum permeability μ_0 and depending on the interparticle separation $\mathbf{r}_{jj'} = \mathbf{r}_{j'} - \mathbf{r}_j$. The Green's tensor is defined such that the real part of the self-interaction at $j = j'$ vanishes. From the steady-state solution of the quantum master equation $\dot{\rho} = \mathrm{i}[\rho, \mathcal{H}_0 + \mathcal{H}_{\text{d-d}} + \mathcal{H}_l] + \mathcal{L}[\rho]$, the dipole amplitudes and thereby the transmitted and reflected fields can be computed (see Supplemental Material [55]). The transmission amplitude of the metasurface for a single Cartesian component $E_{\text{in},\nu}$ is then simply given by [25,26]

$$t_m = 1 + \frac{\mathrm{i}\tilde{\Gamma}(0)/2}{\tilde{\Omega}(0) - \Delta - \mathrm{i}\tilde{\Gamma}(0)/2}, \quad (4)$$

where $\tilde{\Omega}(0) = \sum_j \Omega_{0j}^{\nu\nu}$, $\tilde{\Gamma}(0) = \sum_j \Gamma_{0j}^{\nu\nu}$ describe the dipole-induced collective frequency shift and decay rate arising from the ν transition dipoles. The complex transmission and reflection amplitudes are connected as $t_m = 1 + r_m$ while $|t_m|^2 + |r_m|^2 = 1$. Most notably, if the laser frequency matches the collective metasurface resonance $\omega_l = \omega_\nu + \tilde{\Omega}(0)$, perfect reflection of incoming light is obtained as $|r_m|^2 = 1$. In the following, for the sake of clarity, we proceed with the simplified two-level description. Finally, to obtain a HP mirror, we consider now two copies of metasurfaces separated by a distance ℓ_m, one with dipoles pointing in x direction and one with dipoles pointing in the y direction with a path length difference of $k_l \ell_m = \phi_m = 2\pi n_m + \pi/2$ ($n_m \in \mathbb{N}_0$) between the two polarizations. The combination of these two mirrors is a helicity-preserving mirror. The path length difference leads to a total phase difference of π between the x- and y-polarization components in reflection, thereby reversing the mirror operation which does not conserve helicity for an ordinary mirror. A full transfer matrix calculation showing this can be found in the Supplemental Material [55].

HP cavity.—A HP optical cavity can now be simply implemented by two HP metasurface mirrors separated by a distance ℓ [see Fig. 1(a)]. The two layers making up a HP mirror consist of dipoles with perpendicular dipole orientations, leading to vanishing interactions between the x and y subcavities, which also holds in the near field. For simplicity, we thus continue the discussion for a single cavity while keeping in mind that the actual setup consists of two noninteracting copies. A full discussion for both polarization components can be found in the Supplemental Material [55]. Solving the coupled-dipole equations and neglecting the contributions from all evanescent terms, a

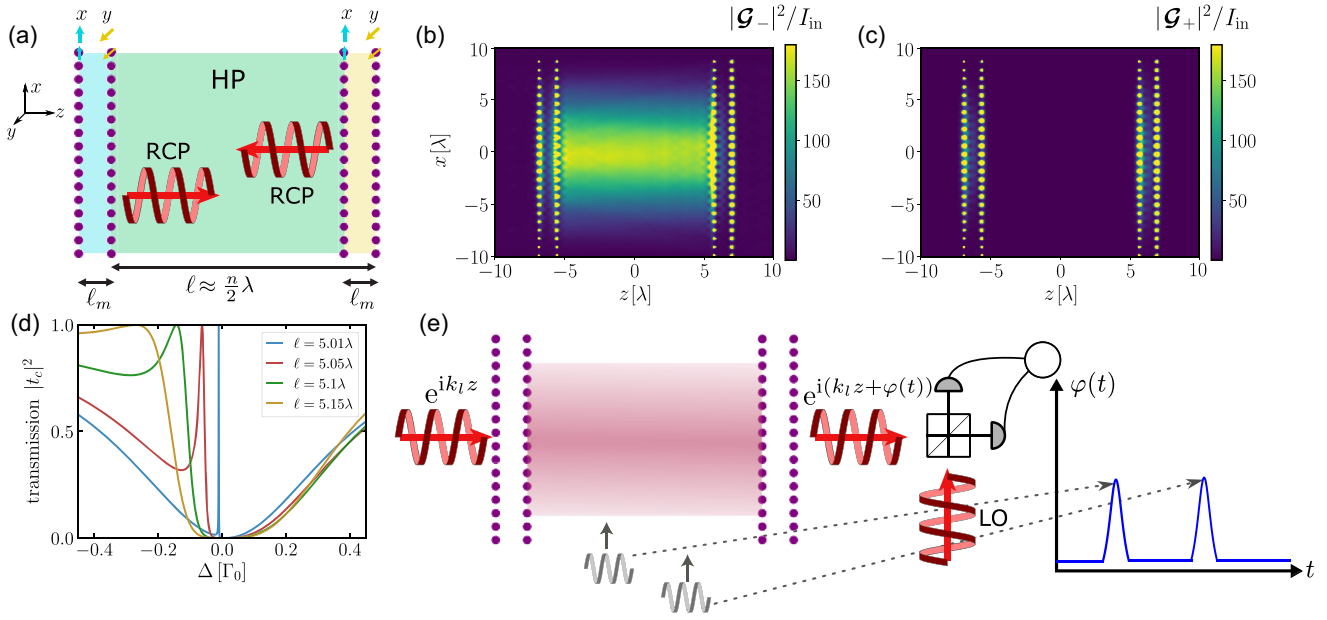

FIG. 1. Helicity-preserving metasurface cavity. (a) A HP metasurface cavity can be constructed with composite mirrors of orthogonal dipole orientation (e.g., along x and y), with an appropriate relative phase separation of $\phi_m = k_l \ell_m = \pi/2 + 2\pi n_m$. (b),(c) Absolute value squared of RS vectors $\mathcal{G}_\pm(\mathbf{R})$ for a cavity length $\ell = 12.505\lambda$, $\ell_m = 5\lambda/4$, for square lattices with lattice spacing $a = 0.8\lambda$ illuminated by RCP light with input polarization vector $\mathbf{E}_{\rm in}^{(+)} = (1, \mathrm{i}, 0)^\top/\sqrt{2}$ close to the cavity resonance. The plots are normalized to the input intensity $I_{\rm in} = |\mathbf{E}_{\rm in}^{(+)}|^2$. The metasurfaces are defined with a finite curvature radius, leading to Gaussian confinement of the mode (beam waist $w_0 = 8\lambda$). (d) Cavity transmission $|t_c|^2$ as a function of the laser detuning Δ for different cavity lengths ℓ. (e) Chiral sensing with HP metasurface cavities: Ideal chiral scatterers passing through a cavity with the same handedness yield a phase shift in the cavity transmission output which can be measured by homodyne detection [local oscillator (LO)] and leads to a phase detection sequence as schematically illustrated in the diagram.

simple expression for the total transmitted field can be obtained as $E^{(+)}(z > \ell) = t_c E_{\rm in}^{(+)} e^{ik_l z}$ with the cavity transmission coefficient (assuming $k_0 \approx k_l$, for derivation see Supplemental Material [55])

$$t_c = \frac{(\Delta - \tilde{\Omega}(0))^2}{\left(\Delta - \tilde{\Omega}(0) + \mathrm{i}\frac{\tilde{\Gamma}(0)}{2}\right)^2 + \frac{\tilde{\Gamma}(0)^2}{4} e^{2ik_l \ell}}. \tag{5}$$

We remark that instead of solving the coupled-dipole equations for the two arrays, the same result can be obtained from classical transfer matrix theory [38,47,60], where the transfer matrix of a single metasurface can be expressed in terms of the mirror polarizability $\zeta_m = -\mathrm{i} r_m/t_m = \tilde{\Gamma}(0)/[2(\tilde{\Omega}(0) - \Delta)]$ as

$$\mathbf{T}_m = \begin{pmatrix} 1 + \mathrm{i}\zeta_m & \mathrm{i}\zeta_m \\ -\mathrm{i}\zeta_m & 1 - \mathrm{i}\zeta_m \end{pmatrix}. \tag{6}$$

The total transfer matrix is then simply obtained as $\mathbf{T} = \mathbf{T}_m \mathbf{T}_f \mathbf{T}_m$ with the free space propagation matrix $\mathbf{T}_f = \mathrm{diag}(e^{ik_l \ell}, e^{-ik_l \ell})$. The condition that the transmission ought to equal unity at the cavity resonance $|t_c|^2 = 1$, yields the following expression for the cavity resonance:

$$\Delta - \tilde{\Omega}(0) = -\frac{\tilde{\Gamma}(0)}{2} \tan(k_l \ell). \tag{7}$$

To demonstrate that the resulting cavity consisting of two HP mirrors indeed preserves the helicity, we compute the Riemann-Silberstein (RS) vectors [61]

$$\mathcal{G}_\pm(\mathbf{R}) = \frac{1}{\sqrt{2}}(\mathbf{E}(\mathbf{R}) \pm \mathrm{i}\mathcal{Z}\mathbf{H}(\mathbf{R})), \tag{8}$$

which describe the combined electromagnetic field of chiral polarization and $\mathcal{Z} = (\epsilon_0 c)^{-1}$ is the vacuum impedance. The absolute value of these quantities is plotted in Figs. 1(b) and 1(c), for RCP light entering the cavity, confirming that the cavity preserves the helicity while also showing a strong field enhancement for this component [62]. The cavity itself is, however, not chiral as *any* elliptical input polarization is supported. The magnetic field $\mathbf{H}(\mathbf{R})$ is determined via Maxwell's equations from the excitations of the electric dipoles on the metasurface as detailed in the Supplemental Material [55].

The transmission profile around the cavity resonance is illustrated in Fig. 1(d) for different cavity lengths for a lattice spacing of $a = 0.8\lambda$, where the dipole-induced collective frequency shift is close to zero, i.e., $\tilde{\Omega}(0) \approx 0$. If the cavity length ℓ exactly matches $n\lambda/2$ ($n \in \mathbb{N}$), the

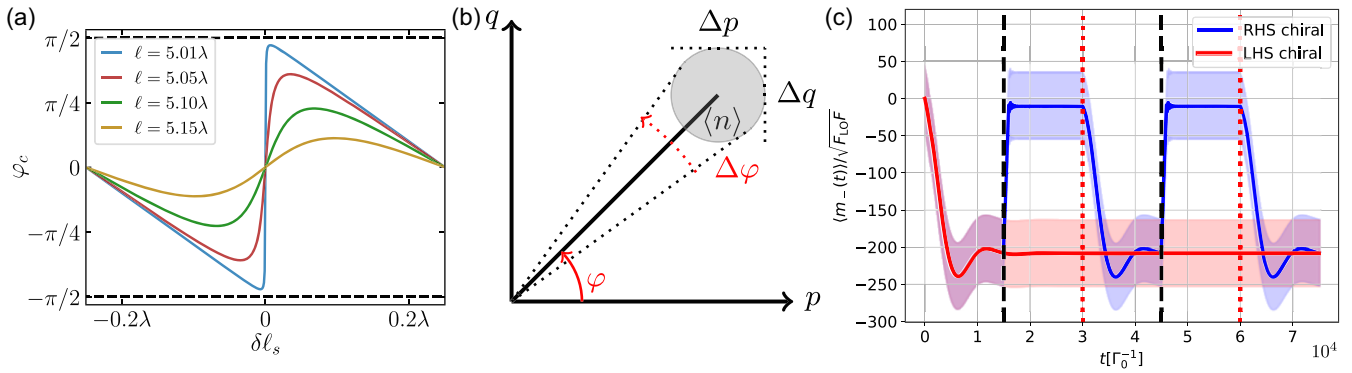

FIG. 2. Chiral sensing.—(a) Cavity phase $\varphi_c = \arg(t_c)$ versus small perturbations of the cavity length $\delta\ell_s$ for different cavity lengths ℓ (square lattice, $a = 0.8\lambda$). For each ℓ, the resonance condition described by Eq. (7) is fulfilled. (b) Illustration of phase uncertainty in phase space for a coherent state. (c) Homodyne detection signal $\langle m_-(t)\rangle$ for (ideal) right- and left-handed chiral scatterers passing through a RCP cavity with corresponding shot noise shown as shaded area. The dashed black line indicates the entry of a particle into the cavity and the dotted red line indicates its exit. In addition, a rotational average was performed as detailed in the Supplemental Material [55]. We have used $\Delta_s = 10\Gamma_0$, $\gamma_s = \Gamma_0$, with an average of one photon within the time interval Γ_0^{-1}, i.e., $F = \Gamma_0$, an integration time of $T\Gamma_0 = 2000$ and a detuning of $\Delta = \Gamma_0/100$.

cavity resonance coincides with the resonance of an individual layer and no transmission is obtained as all the light is reflected. If ℓ becomes slightly larger, a narrow transmission window opens up as the mirrors and the cavity now possess different resonance frequencies. Further increasing the cavity length leads to a strongly asymmetric Fano-type profile with a larger linewidth and the cavity resonance drifting towards infinity for $\ell \to (n + \frac{1}{2})\lambda/2$. Once the next multiple of $\lambda/2$ is approached, the cavity linewidth becomes narrow again and the cavity resonance shifts towards $\omega_\nu + \tilde{\Omega}(0)$ as $\tan(k_l\ell) \to 0$. The distance between the zero and the maximum of the transmission can be used as a measure for the cavity linewidth $\kappa = \tilde{\Gamma}(0)|\tan(k_l\ell)|$. We present a coupled-modes theory for the input-output description of cavities made from quantum metasurface mirrors in the Supplemental Material [55].

Chiral sensing.—We now consider the scenario depicted in Fig. 1(e) where chiral scatterers with radiative linewidth γ_s are sent through the cavity. We assume the resonance of the scatterers ω_s to be far-detuned from the cavity resonance $|\Delta_s| \gg |\Delta_c|, \gamma_s$ with $\Delta_{s/c} = \omega_l - \omega_{s/c}$. In this case, the effect of a scatterer with the same helicity as the cavity is to increase the path length of light passing through the cavity and thereby shift the cavity length by a small amount $\delta\ell_s = -\arctan(\gamma_s/2\Delta_s)/k_l$ (for derivation see Supplemental Material [55]), such that the total effective cavity length is now given by $\ell + \delta\ell_s$. Because of the quick phase switch around the cavity resonance for cavity lengths close to $n\lambda/2$, a small perturbation of the cavity length can lead to a considerable phase shift of the cavity transmission [see Fig. 2(a)].

One can proceed to compute the relative phase change in the cavity transmission between lengths ℓ and $\ell + \delta\ell_s$ on the cavity resonance (assuming $\ell \approx n\lambda/2$)

$$\varphi = \arg \frac{t_c(\ell + \delta\ell_s)}{t_c(\ell)}\bigg|_{\mathrm{res},\ell \approx n\frac{\lambda}{2}} \approx \arctan\left(\cot(2k_l\delta\ell_s)\right), \tag{9}$$

which reaches a value of $\pi[\theta(k_l\delta\ell_s) - 1/2]$ as $\delta\ell_s \to 0$, implying a phase jump from $-\pi/2$ to $\pi/2$ around the cavity resonance for lengths close to $n\lambda/2$ [$\theta(x)$ is the Heaviside function]. If the cavity length departs from $n\lambda/2$, the cavity linewidth increases and the phase shift gets diminished, as illustrated in Figs. 1(d) and 2(a).

An experimental setup to measure this phase is homodyne detection as illustrated in Fig. 1(e), where the phase between a local oscillator (for instance, obtained from beam splitting the input field) is compared to the phase of the output field. Suppose we consider a signal beam with which we drive the cavity $\alpha(t) = \sqrt{F}\exp(-i\omega_l t + i\theta)$ and the local oscillator field $\alpha_{LO}(t) = \sqrt{F_{LO}}\exp(-i\omega_l t + i\theta_{LO})$ with intensities (number of photons per unit of time) F and F_{LO}. Then considering homodyne detection for a Fabry-Pérot cavity leads to an uncertainty in the measured phase for an integration time T of the measurement and a quantum efficiency η_Q, which is encoded in the intensity difference m_- with variance $(\Delta m_-)^2_{\mathrm{res}} = \eta_Q T F_{LO}$ and expectation value (assuming the phase variation to happen on a timescale much slower than the optical frequency)

$$\langle m_-(t,T)\rangle = 2\eta_Q\sqrt{FF_{LO}}|t_c|\int_t^{t+T} dt' \sin\left(\varphi(t')\right). \tag{10}$$

Here, we have approximated that $F_{LO} \gg F$ and have taken $\theta + \theta_{LO} = 2\pi n$, which can be obtained by phase matching the local oscillator and the signal beam. Since the cavity is a linear element, the resulting phase uncertainty [see Fig. 2(b)] is independent of any cavity properties and only depends on the properties of the state of the incoming beam, which is assumed to be classical for this calculation.

As an alternative to describing the passage of particles through the cavity with transfer matrix theory, the dipole theory can be extended to include the presence of an additional chiral scatterer which can be represented by coupled electric and magnetic dipoles (see Supplemental Material [55]). These equations of motion are simulated in Fig. 2(c) for right- and left-handed scatterers (RHS and LHS) entering a RCP cavity, showing a clear distinction in the resulting signal. Here, the classical shot noise of a coherent input field is used to estimate the phase error for a homodyne detection.

Let us finally briefly discuss the applicability of the chiral sensing scheme to the discrimination of molecular enantiomers. Chiral molecules are, in general, not perfect chiral scatterers. This is manifested in the fact that their circular dichroism $\mathrm{CD} = (A_+ - A_-)/(A_+ + A_-)$, i.e., the difference in absorbance between RCP and LCP light, is not unity but some small finite value. This implies that the assumption of coupling to only a single polarization component is unrealistic. Instead, both enantiomers will lead to small differential shifts in optical path length. Aside from the absolute magnitude of this change in path length, however, the presented strategy retains generality and the applicability is a question of detailed system parameters.

Conclusions and outlook.—We have proposed a novel approach for chiral sensing based on the interferometric detection of phase shifts in HP metasurface cavities. In a first step, we have shown that HP mirrors and cavities can be created from stacked quantum metasurfaces with orthogonal dipole orientation. We then proposed to use these narrow-linewidth HP cavity modes for the optical sensing of chiral scatterers by discussing how the phase of the output field is modified by an off-resonant scatterer passing through the cavity. We also discussed briefly the applicability to the discrimination of molecular enantiomers. Our approach constitutes a fully optical approach to chiral sensing in the linear regime as compared to other approaches relying on nonlinear techniques [20]. Furthermore, it does not require strong coupling or resonance between the scatterers and the cavity mode in contrast to other recent treatments of cavity-based enantiomer discrimination [17]. We provide a discussion of possible errors leading to, e.g., mixing of helicities in the Supplemental Material [55]. We have previously discussed derogating effects such as motion, vacancies, and nonlinearities for single metasurfaces in Ref. [52].

We also remark that, in addition to the use proposed in this Letter, layered metasurfaces can enable a host of other applications. For instance, stacking many of these layers leads to Bragg-mirror physics which could be used to tailor the frequency windows of optical elements based on quantum metasurfaces. Even more general polarization structures of the cavity mode, such as Faraday cavities [22], might also be implementable.

We acknowledge fruitful discussions with L. Mauro and J. Fregoni which led to the initial idea for this project. This work was supported by the Max Planck Society and the Deutsche Forschungsgemeinschaft (DFG, German Research Foundation)—ID 429529648—TRR 306 QuCoLiMa ("Quantum Cooperativity of Light and Matter").

[1] M. M. Coles and D. L. Andrews, Chirality and angular momentum in optical radiation, Phys. Rev. A **85**, 063810 (2012).
[2] S. M. Barnett, R. P. Cameron, and A. M. Yao, Duplex symmetry and its relation to the conservation of optical helicity, Phys. Rev. A **86**, 013845 (2012).
[3] A. Aiello, Helicity, chirality, and spin of optical fields without vector potentials, Phys. Rev. A **106**, 043519 (2022).
[4] E. Plum and N. I. Zheludev, Chiral mirrors, Appl. Phys. Lett. **106** (2015).
[5] M. Hentschel, M. Schäferling, X. Duan, H. Giessen, and N. Liu, Chiral plasmonics, Sci. Adv. **3**, e1602735 (2017).
[6] B. Semnani, J. Flannery, R. Al Maruf, and M. Bajcsy, Spin-preserving chiral photonic crystal mirror, Light Sci. Appl. **9**, 23 (2020).
[7] J. Feis, D. Beutel, J. Köpfler, X. Garcia-Santiago, C. Rockstuhl, M. Wegener, and I. Fernandez-Corbaton, Helicity-preserving optical cavity modes for enhanced sensing of chiral molecules, Phys. Rev. Lett. **124**, 033201 (2020).
[8] M. V. Gorkunov, A. A. Antonov, and Y. S. Kivshar, Metasurfaces with maximum chirality empowered by bound states in the continuum, Phys. Rev. Lett. **125**, 093903 (2020).
[9] K. Voronin, A. S. Taradin, M. V. Gorkunov, and D. G. Baranov, Single-handedness chiral optical cavities, ACS Photonics **9**, 2652 (2022).
[10] H. S. Khaliq, A. Nauman, J.-W. Lee, and H.-R. Kim, Recent progress on plasmonic and dielectric chiral metasurfaces: Fundamentals, design strategies, and implementation, Adv. Opt. Mater. **11**, 2300644 (2023).
[11] Y. Chen, H. Deng, X. Sha, W. Chen, R. Wang, Y.-H. Chen, D. Wu, J. Chu, Y. S. Kivshar, S. Xiao, and C.-W. Qiu, Observation of intrinsic chiral bound states in the continuum, Nature (London) **613**, 474 (2023).
[12] Y. Tang and A. E. Cohen, Optical chirality and its interaction with matter, Phys. Rev. Lett. **104**, 163901 (2010).
[13] P. Scott, X. Garcia-Santiago, D. Beutel, C. Rockstuhl, M. Wegener, and I. Fernandez-Corbaton, On enhanced sensing of chiral molecules in optical cavities, Appl. Phys. Rev. **7**, 041413 (2020).
[14] E. Mohammadi, K. L. Tsakmakidis, A. N. Askarpour, P. Dehkhoda, A. Tavakoli, and H. Altug, Nanophotonic platforms for enhanced chiral sensing, ACS Photonics **5**, 2669 (2018).
[15] C. Genet, Chiral light-chiral matter interactions: An optical force perspective, ACS Photonics **9**, 319 (2022).
[16] L. Mauro, J. Fregoni, J. Feist, and R. Avriller, Chiral discrimination in helicity-preserving Fabry-Pérot cavities, Phys. Rev. A **107**, L021501 (2023).

[17] R. R. Riso, L. Grazioli, E. Ronca, T. Giovannini, and H. Koch, Strong coupling in chiral cavities: Nonperturbative framework for enantiomer discrimination, Phys. Rev. X **13**, 031002 (2023).
[18] L. Nahon, G. A. Garcia, and I. Powis, Valence shell one-photon photoelectron circular dichroism in chiral systems, J. Electron Spectrosc. Relat. Phenom. **204**, 322 (2015).
[19] D. Patterson, M. Schnell, and J. M. Doyle, Enantiomer-specific detection of chiral molecules via microwave spectroscopy, Nature (London) **497**, 475 (2013).
[20] D. Ayuso, A. F. Ordonez, and O. Smirnova, Ultrafast chirality: The road to efficient chiral measurements, Phys. Chem. Chem. Phys. **24**, 26962 (2022).
[21] R. Naaman and D. H. Waldeck, Spintronics and chirality: Spin selectivity in electron transport through chiral molecules, Annu. Rev. Phys. Chem. **66**, 263 (2015).
[22] H. Hübener, U. De Giovannini, C. Schäfer, J. Andberger, M. Ruggenthaler, J. Faist, and A. Rubio, Engineering quantum materials with chiral optical cavities, Nat. Mater. **20**, 438 (2021).
[23] C. Schäfer and D. G. Baranov, Chiral polaritonics: Analytical solutions, intuition, and use, J. Phys. Chem. Lett. **14**, 3777 (2023).
[24] J. Rui, D. Wei, A. Rubio-Abadal, S. Hollerith, J. Zeiher, D. M. Stamper-Kurn, C. Gross, and I. Bloch, A subradiant optical mirror formed by a single structured atomic layer, Nature (London) **583**, 369 (2020).
[25] R. J. Bettles, S. A. Gardiner, and C. S. Adams, Enhanced optical cross section via collective coupling of atomic dipoles in a 2D array, Phys. Rev. Lett. **116**, 103602 (2016).
[26] E. Shahmoon, D. S. Wild, M. D. Lukin, and S. F. Yelin, Cooperative resonances in light scattering from two-dimensional atomic arrays, Phys. Rev. Lett. **118**, 113601 (2017).
[27] K. E. Ballantine and J. Ruostekoski, Optical magnetism and Huygens' surfaces in arrays of atoms induced by cooperative responses, Phys. Rev. Lett. **125**, 143604 (2020).
[28] R. Alaee, B. Gurlek, M. Albooyeh, D. Martín-Cano, and V. Sandoghdar, Quantum metamaterials with magnetic response at optical frequencies, Phys. Rev. Lett. **125**, 063601 (2020).
[29] K. E. Ballantine and J. Ruostekoski, Cooperative optical wavefront engineering with atomic arrays, Nanophotonics **10**, 1901 (2021).
[30] R. J. Bettles, J. Minar, C. S. Adams, I. Lesanovsky, and B. Olmos, Topological properties of a dense atomic lattice gas, Phys. Rev. A **96**, 041603(R) (2017).
[31] J. Perczel, J. Borregaard, D. E. Chang, H. Pichler, S. F. Yelin, P. Zoller, and M. D. Lukin, Photonic band structure of two-dimensional atomic lattices, Phys. Rev. A **96**, 063801 (2017).
[32] J. Perczel, J. Borregaard, D. E. Chang, H. Pichler, S. F. Yelin, P. Zoller, and M. D. Lukin, Topological quantum optics in two-dimensional atomic arrays, Phys. Rev. Lett. **119**, 023603 (2017).
[33] R. J. Bettles, M. D. Lee, S. A. Gardiner, and J. Ruostekoski, Quantum and nonlinear effects in light transmitted through planar atomic arrays, Commun. Phys. **3**, 141 (2020).
[34] C. D. Parmee and J. Ruostekoski, Bistable optical transmission through arrays of atoms in free space, Phys. Rev. A **103**, 033706 (2021).
[35] M. Moreno-Cardoner, D. Goncalves, and D. E. Chang, Quantum nonlinear optics based on two-dimensional Rydberg atom arrays, Phys. Rev. Lett. **127**, 263602 (2021).
[36] C. C. Rusconi, T. Shi, and J. I. Cirac, Exploiting the photonic nonlinearity of free-space subwavelength arrays of atoms, Phys. Rev. A **104**, 033718 (2021).
[37] K. Srakaew, P. Weckesser, S. Hollerith, D. Wei, D. Adler, I. Bloch, and J. Zeiher, A subwavelength atomic array switched by a single Rydberg atom, Nat. Phys. **19**, 714 (2023).
[38] S. P. Pedersen, L. Zhang, and T. Pohl, Quantum nonlinear metasurfaces from dual arrays of ultracold atoms, Phys. Rev. Res. **5**, L012047 (2023).
[39] D. Plankensteiner, L. Ostermann, H. Ritsch, and C. Genes, Selective protected state preparation of coupled dissipative quantum emitters, Sci. Rep. **5**, 16231 (2015).
[40] G. Facchinetti, S. D. Jenkins, and J. Ruostekoski, Storing light with subradiant correlations in arrays of atoms, Phys. Rev. Lett. **117**, 243601 (2016).
[41] M. T. Manzoni, M. Moreno-Cardoner, A. Asenjo-Garcia, J. V. Porto, A. V. Gorshkov, and D. E. Chang, Optimization of photon storage fidelity in ordered atomic arrays, New J. Phys. **20**, 083048 (2018).
[42] A. Grankin, P. O. Guimond, D. V. Vasilyev, B. Vermersch, and P. Zoller, Free-space photonic quantum link and chiral quantum optics, Phys. Rev. A **98**, 043825 (2018).
[43] P.-O. Guimond, A. Grankin, D. V. Vasilyev, B. Vermersch, and P. Zoller, Subradiant Bell states in distant atomic arrays, Phys. Rev. Lett. **122**, 093601 (2019).
[44] R. Bekenstein, I. Pikovski, H. Pichler, E. Shahmoon, S. F. Yelin, and M. D. Lukin, Quantum metasurfaces with atom arrays, Nat. Phys. **16**, 676 (2020).
[45] S. Choudhary, R. W. Boyd, and J. E. Sipe, Dark and bright modes, and their coherent control in dipolar metasurface bilayers, Phys. Rev. A **107**, 023521 (2023).
[46] W. Zhou, D. Zhao, Y.-C. Shuai, H. Yang, S. Chuwongin, A. Chadha, J.-H. Seo, K. X. Wang, V. Liu, Z. Ma, and S. Fan, Progress in 2D photonic crystal Fano resonance photonics, Prog. Quantum Electron. **38**, 1 (2014).
[47] O. Cernotík, A. Dantan, and C. Genes, Cavity quantum electrodynamics with frequency-dependent reflectors, Phys. Rev. Lett. **122**, 243601 (2019).
[48] E. V. Denning, J. Iles-Smith, and J. Mork, Quantum light-matter interaction and controlled phonon scattering in a photonic Fano cavity, Phys. Rev. B **100**, 214306 (2019).
[49] J. M. Fitzgerald, S. K. Manjeshwar, W. Wieczorek, and P. Tassin, Cavity optomechanics with photonic bound states in the continuum, Phys. Rev. Res. **3**, 013131 (2021).
[50] M. S. Bin-Alam, O. Reshef, Y. Mamchur, M. Z. Alam, G. Carlow, J. Upham, B. T. Sullivan, J.-M. Ménard, M. J. Huttunen, R. W. Boyd, and K. Dolgaleva, Ultra-high-Q resonances in plasmonic metasurfaces, Nat. Commun. **12**, 974 (2021).
[51] A. E. Miroshnichenko, S. Flach, and Y. S. Kivshar, Fano resonances in nanoscale structures, Rev. Mod. Phys. **82**, 2257 (2010).
[52] N. S. Baßler, M. Reitz, K. P. Schmidt, and C. Genes, Linear optical elements based on cooperative subwavelength emitter arrays, Opt. Express **31**, 6003 (2023).
[53] A. Jaber, M. Reitz, A. Singh, A. Maleki, Y. Xin, B. Sullivan, K. Dolgaleva, R. W. Boyd, C. Genes, and J.-M. Ménard,

Hybrid THz architectures for molecular polaritonics, arXiv:2304.03654.

[54] P. Back, S. Zeytinoglu, A. Ijaz, M. Kroner, and A. Imamoğlu, Realization of an electrically tunable narrow-bandwidth atomically thin mirror using monolayer $MoSe_2$, Phys. Rev. Lett. **120**, 037401 (2018).

[55] See Supplemental Material at http://link.aps.org/supplemental/10.1103/PhysRevLett.132.043602 for detailed derivations on coupled-dipole theory, transfer matrix formalism, coupled-modes theory for hybrid cavities, and homodyne detection. Additionally, it includes Refs. [56–59].

[56] L. Novotny and B. Hecht, *Principles of Nano-Optics* (Cambridge University Press, Cambridge, England, 2006), 10.1017/CBO9780511813535.

[57] C. Viviescas and G. Hackenbroich, Field quantization for open optical cavities, Phys. Rev. A **67**, 013805 (2003).

[58] D. P. Craig and T. Thirunamachandran, *Molecular Quantum Electrodynamics: An Introduction to Radiation-Molecule Interactions* (Courier Corporation, Mineola, 1998).

[59] R. Loudon, *The Quantum Theory of Light* (Oxford University Press, Oxford, 2000).

[60] M. Reitz, C. Sommer, and C. Genes, Cooperative quantum phenomena in light-matter platforms, PRX Quantum **3**, 010201 (2022).

[61] I. Bialynicki-Birula and Z. Bialynicka-Birula, The role of the Riemann-Silberstein vector in classical and quantum theories of electromagnetism, J. Phys. A Math. Theor. **46**, 053001 (2013).

[62] $\mathcal{G}_+$ and $\mathcal{G}_-$ describes the LCP (RCP) component.